Published September 14, 2015

Structures of the yeast dynamin-like GTPase Sey1p provide insight into homotypic ER fusion

Liming Yan,[1]* Sha Sun,[2]* Wei Wang,[1,4] Juanming Shi,[2] Xiaoyu Hu,[2] Shiyan Wang,[4] Dan Su,[5] Zihe Rao,[1,3,6] Junjie Hu,[2,3] and Zhiyong Lou[1,6]

[1]School of Medicine, Tsinghua University, Beijing, China 100084
[2]Department of Genetics and Cell Biology, College of Life Sciences, Nankai University and Tianjin Key Laboratory of Protein Sciences, Tianjin, China 300071
[3]National Laboratory of Macromolecules, Institute of Biophysics, Chinese Academy of Science, Beijing, China 100101
[4]State Key Laboratory of Cotton Biology, Key Laboratory of Plant Stress Biology, Henan University, Kaifeng, China 475004
[5]Collaborative Innovation Center for Biotherapy, State Key Laboratory of Biotherapy and Cancer Center, West China Hospital, West China Medical School, Sichuan University, Chengdu, China 610041[6]Collaborative Innovation Center for Biotherapy, West China Hospital, West China Medical School, Sichuan University, Chengdu, China 610041

Homotypic membrane fusion of the endoplasmic reticulum is mediated by dynamin-like guanosine triphosphatases (GTPases), which include atlastin (ATL) in metazoans and Sey1p in yeast. In this paper, we determined the crystal structures of the cytosolic domain of Sey1p derived from *Candida albicans*. The structures reveal a stalk-like, helical bundle domain following the GTPase, which represents a previously unidentified configuration of the dynamin superfamily. This domain is significantly longer than that of ATL and critical for fusion. Sey1p forms a side-by-side dimer in complex with GMP-PNP or GDP/AlF_4^- but is monomeric with GDP. Surprisingly, Sey1p could mediate fusion without GTP hydrolysis, even though fusion was much more efficient with GTP. Sey1p was able to replace ATL in mammalian cells, and the punctate localization of Sey1p was dependent on its GTPase activity. Despite the common function of fusogenic GTPases, our results reveal unique features of Sey1p.

Introduction

The ER network consists of a continuous membrane system of tubules and sheets (Shibata et al., 2006). ER membranes are interconnected by homotypic fusion to maintain a reticular pattern and proper functioning. In metazoans, fusion is mediated by a class of dynamin-like GTPases called atlastin (ATL; Hu et al., 2009; Orso et al., 2009). In other eukaryotic organisms lacking ATL, a similar class of GTPases, including Sey1p in *Saccharomyces cerevisiae* (Hu et al., 2009; Anwar et al., 2012) and RHD3 in *Arabidopsis thaliana* (Zhang et al., 2013), has been identified. Deletion of Sey1p or depletion of ATL proteins in cells results in unbranched ER (Hu et al., 2009), delayed ER fusion (Anwar et al., 2012), or even ER fragmentation (Orso et al., 2009). When purified and reconstituted in vitro, members of both classes have been shown to mediate membrane fusion (Orso et al., 2009; Bian et al., 2011; Anwar et al., 2012; Zhang et al., 2013).

GTPase-based ER fusogens play critical physiological roles. In *Candida albicans*, deletion of Sey1p results in decreased virulence (Yamada-Okabe and Yamada-Okabe, 2002). In *A. thaliana*, lack of RHD3 leads to short and wavy root hairs and cell expansion defects (Schiefelbein and Somerville, 1990; Chen et al., 2011; Stefano et al., 2012), and the deletion of another family member causes lethality (Zhang et al., 2013). In *Drosophila melanogaster* and *Danio rerio*, depletion of ATL causes neuronal defects (Lee et al., 2008, 2009). In humans, mutations in ATL1, the dominant form of ATL in the central nervous system, are tightly associated with hereditary spastic paraplegia, a neurodegenerative disease characterized by axon shortening in corticospinal motor neurons and progressive spasticity and weakness of the lower limbs (Zhao et al., 2001; Salinas et al., 2008).

ATL, Sey1p, and RHD3 are anchored in the ER membrane by two closely spaced transmembrane (TM) segments, exposing both termini to the cytosol. The mechanism for homotypic ER fusion has been partially unveiled using ATLs (Hu et al., 2011; Lin et al., 2012). It is very different from SNARE or viral protein-mediated fusion. Recent structural and biochemical studies indicate that the GTPase domain of ATL forms a dimer upon GTP binding, initiating contact between apposing membranes (Bian et al., 2011; Byrnes and Sondermann, 2011). The region following the GTPase domain is a three-helix bundle (3HB) and can dock to its own GTPase domain or that of a neighboring molecule, undergoing major conformational changes during the GTP cycle to drive fusion (Bian et al., 2011;

*L. Yan and S. Sun contributed equally to this paper.

Correspondence to Junjie Hu: huj@ibp.ac.cn; or Zhiyong Lou: louzy@mail.tsinghua.edu.cn

Abbreviations used in this paper: 3HB, three-helix bundle; ATL, atlastin; AUC, analytical ultracentrifugation; BDLP, bacterial dynamin-like protein; NBD, nitrobenzoxadiazole; PEG, polyethylene glycol; TM, transmembrane.

Supplemental Material can be found at:
http://jcb.rupress.org/content/suppl/2015/09/10/jcb.201502078.DC1.html

The Rockefeller University Press $30.00
J. Cell Biol. Vol. 210 No. 6 961–972
www.jcb.org/cgi/doi/10.1083/jcb.201502078

Published September 14, 2015

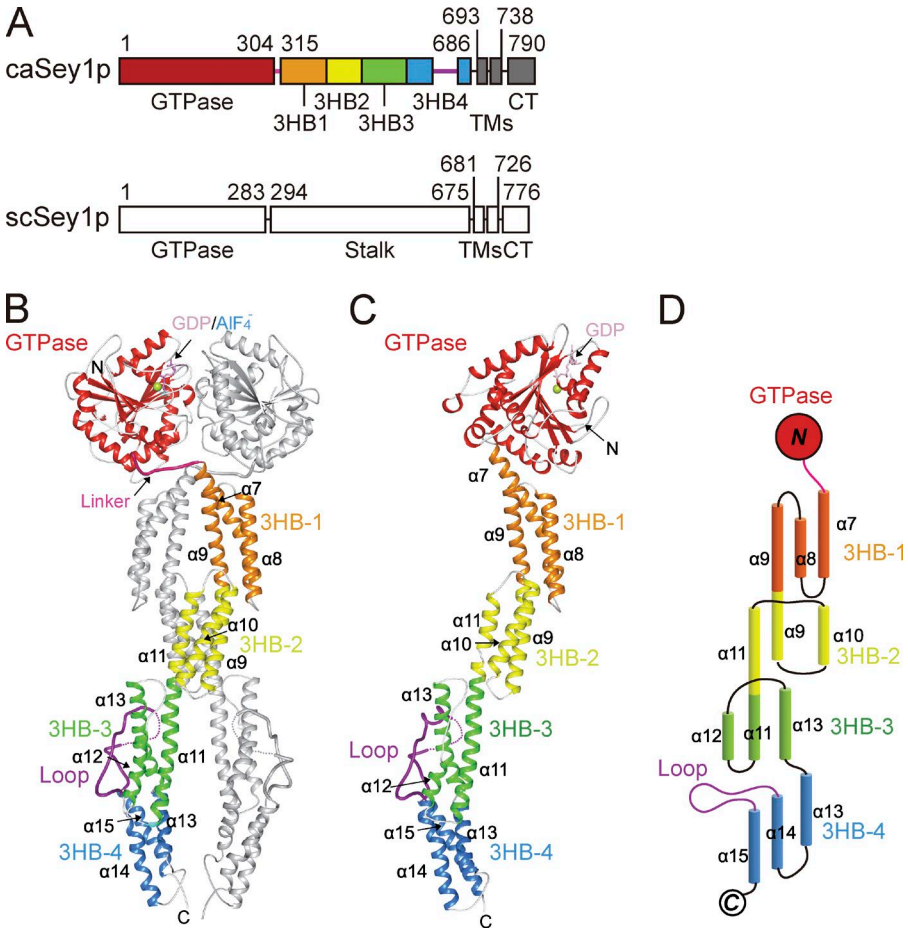

Figure 1. **Structures of the cytosolic domain of Sey1p.** (A) Scheme showing the domains of Sey1p from *C. albicans* (caSey1p) and *S. cerevisiae* (scSey1p). Residue numbers for each domain are indicated. The domains of caSey1p are colored, respectively. 3HB, three-helix bundle; TMs, transmembrane segments; CT, cytosolic tail. (B) Structure of the GDP/AlF_4^--bound form of caSey1p. The protomers in the dimer are shown in colored (as in A) and gray cartoon representation. The linker between the GTPase and stalk domain and the long loop in the stalk domain are highlighted. GDP is shown in pink stick representation, AlF_4^- is in cyan sticks, and magnesium ion is shown as a lime sphere. The 3HBs in the stalk domain are numbered, and the secondary structure elements are labeled. (C) As in B, but for structure of caSey1p crystallized with GDP. (D) A topology plot of the stalk domain, colored as in A.

Byrnes et al., 2013). Membrane tethering has also been shown to require continuous GTP hydrolysis of ATL (Saini et al., 2014; Liu et al., 2015). Fusion is facilitated by a membrane-binding amphipathic helix in the C-terminal tail and the TM segments (Liu et al., 2012; Faust et al., 2015).

Identical membrane topology and conserved signature motifs in the GTPase domains of ATL and Sey1p suggest that Sey1p may behave similarly to ATL during membrane fusion. However, the predicted helical domain between the GTPase domain and TM segments is much longer (~300 amino acids more) in Sey1p compared with ATL. Furthermore, Sey1p is concentrated in punctae along ER tubules, sometimes at three-way junctions of tubules, whereas ATL1 is mostly distributed evenly on the ER membranes (Hu et al., 2009). Therefore, it is unclear whether Sey1p acts the same way as ATL.

Here, we elucidate how Sey1p mediates homotypic membrane fusion. The proposed mechanism demonstrates a common scheme for fusion mediated by dynamin-like GTPases and reveals that the stalk domain of Sey1p possesses unique functional features.

Results

Crystal structures of the cytosolic domain of Sey1p

To investigate the mechanism of Sey1p-mediated membrane fusion, we determined the structures of the cytosolic domains (cytSey1p) of Sey1p from *C. albicans* (caSey1p). caSey1p shares 43% sequence identity with Sey1p from *S. cerevisiae* (scSey1p; see Fig. S1 A for sequence alignment). Residues 1–692 (truncation before the first TM region; Fig. 1 A) were expressed in *Escherichia coli*, purified, and crystallized first as an orthorhombic form in the presence of GDP plus AlF_4^- (GDP/AlF_4^-). A structure at 2.8-Å resolution was determined by single anomalous diffraction (Table 1), and an electron density map of the nucleotide is shown in Fig. S2 A. Only one caSey1p molecule was present in the asymmetric unit, but a crystallographic dimer occurred along one of the twofold symmetry axes, similar to the hexagonal crystal form of human ATL1 (hsATL1, form 1; Fig. S1 B).

CytSey1p consists of an N-terminal GTPase domain and a long, stalk-like, helical domain connected by a linker region (Fig. 1 B). In the dimer, the GTPase domains interact with one another in such a way that the nucleotide binding sites face each other. The linker regions of the two Sey1p molecules cross one another, allowing a close association of the tops of the stalk domains. The stalk domain is composed of four 3HBs, with the last helix of each bundle extending into the first helix of the next bundle (see Fig. 1 D for topology). The first 3HB (3HB-1) is positioned under the GTPase domain of the pairing protomer. If Sey1p ended here, it would resemble the configuration of the crossover dimer of hsATL1 (form 1; Fig. S1, B and C). The second and third 3HBs (3HB-2 and -3) pivot around each other, so that the last 3HB (3HB-4) remains on the same side as the GTPase domain. 3HB-4 is poorly ordered in general; a partially disordered long loop (residue 615–660) is found between its second and third helices.

Nucleotide-dependent dimerization has been observed with many dynamin-like GTPases (GTPase dimer and Bian et

Published September 14, 2015

al., 2011), but the configuration of the Sey1p stalk domain has not been previously identified. The scale of the domain is comparable to that of bacterial dynamin-like protein (BDLP) and is longer than Dynamin-1 or human guanylate-binding protein 1 (GBP1; Fig. S1 C). In BDLP structures, the stalk domain is composed of two four-helix bundles connected by a flexible hinge (Low and Löwe, 2006; Low et al., 2009). Major conformational changes, namely bending around the hinge, have been proposed for BDLP. In Dynamin-1 structures, the stalk consists of the bundle signaling element and one four-helix bundle, and it plays critical role in oligomerization (Faelber et al., 2011; Ford et al., 2011). The stalk of GBP1 starts with two 3HBs arranged similarly as 3HB-1 and -2 in Sey1p, followed by one long helix that reaches back to the bottom of the GTPase domain (Ghosh et al., 2006). Unlike Sey1p, the stalk domains of BDLP, GBP1, and Dynamin-1 interact extensively with their GTPase domains, suggesting that the GTPase–stalk linkage may have different roles in these proteins.

The same crystal form was obtained when GMP-PNP, a nonhydrolyzable analogue of GTP, was added during purification and crystallization. Overall, the Sey1p structure in GMP-PNP is similar to that of GDP/AlF_4^-, with a root mean square deviation of only 0.3709 Å (Fig. S1 C). In contrast, a different conformation of cytSey1p was observed when the protein was crystallized with GDP (Fig. 1 C). This structure was determined from monoclinic crystals at 2.3-Å resolution using molecular replacement with the GDP/AlF_4^- structure as a search model (Table 1). One Sey1p molecule is found in each asymmetric unit, but unlike the first structure, the stalk domain (mainly 3HB-1) is associated with the GTPase domain of the same molecule. In one of the crystallographic dimers, the GTPase domain of another Sey1p molecule comes in close proximity (Fig. S1 E). Such a crystallographic "dimer" would be reminiscent of form 2 of hsATL1 (Fig. S1 B), in which the 3HBs point in opposite directions and the GTPase domains form a dimer interface of 670 $Å^2$. However, this Sey1p "dimer" buries only 455 $Å^2$ of total surface area, suggesting less substantial contact between the two GTPase domains of the symmetry mates. These results imply that, despite the overall structural similarity between Sey1p and ATL, these proteins likely undergo nucleotide-dependent dimerization differently.

Nucleotide binding and GTP hydrolysis

The GTPase domain of caSey1p folds in a similar manner as other dynamin-like proteins. It is composed of a central β sheet surrounded by six α helices. The nucleotide at the active site is coordinated mainly by a magnesium ion and four signature motifs: the P-loop (G1, β1–α1), the switch 1 region (G2, α1–β2), the switch 2 region (G3, β3–α2), and the G4 motif (after β5; Fig. S2 B). Most residues involving GTP binding are conserved between Sey1p and ATLs (Fig. S2 B). The two residues of ca-

Table 1. **Data collection and refinement statistics**

Parameters (data collection statistics)	GDP/AlF_4^-		GDP	GMP-PNP
	SeMet	Native		
Cell parameters				
a (Å)	75.2	76.27	228.1	76.6
b (Å)	120.6	120.5	43.6	120.9
c (Å)	190.1	190.2	97.6	190.5
α, β, γ (°)	90.0, 90.0, 90.0	90.0, 90.0, 90.0	90.0, 108.1, 90.0	90.0, 90.0, 90.0
Space group	$I2_12_12_1$	$I2_12_12_1$	C2	$I2_12_12_1$
Wavelength used (Å)	0.9792	1.0000	1.0000	1.0000
Resolution (Å)	50.00 (3.05) – 3.00	50.00 (2.85) – 2.80	50.00 (2.42) – 2.30	50.00 (2.86) – 2.80
No. of all reflections	120307 (5,755)	224,007 (6,499)	122,150 (18,308)	139,072 (5,654)
No. of unique reflections	17,527 (872)	21,774 (942)	40,802 (5,930)	19,897 (912)
Completeness (%)	98.7(99.0)	99.0 (87.5)	99.1 (99.4)	99.5 (94.7)
Average I/σ (I)	58.3 (24.4)	43.9 (4.4)	10.2 (2.3)	27.2 (2.9)
R_{merge} (%)[a]	5.7 (10.8)	8.9 (45.2)	5.3 (44.3)	9.3 (58.6)
Refinement statistics				
No. of reflections used (σ(F) > 0)	20,651		38,752	18,876
R_{work} (%)[b]	25.3		22.0	24.4
R_{free} (%)[b]	30.0		29.8	30.3
High resolution shell of R_{free} (%)[b]	45.0		36.9	40.0
High resolution shell of R_{work} (%)[b]	35.0		33.3	33.2
r.m.s.d. bond distance (Å)	0.018		0.015	0.013
r.m.s.d. bond angle (°)	2.000		1.852	1.695
Average B-value ($Å^2$)	86.6		69.2	54.7
No. of protein atoms	5,446		5,327	5,348
No. of ligand atoms	34		58	66
No. of solvent atoms	126		146	22
Ramachandran plot				
Res. in favored regions (%)	93.8		96.8	92.8
Res. in generously allowed regions (%)	5.5		3.0	5.9
Res. in disallowed regions (%)	0.7		1	1.2

Numbers in parentheses are corresponding values for the highest resolution shell. r.m.s.d., root-mean-square deviation; Res., residues.
[a]$R_{merge} = \Sigma_h\Sigma_i ||I_{ih}-<I_h>|/\Sigma_h\Sigma_i <I_h>$, where $<I_h>$ is the mean of the observations I_{ih} of reflection h.
[b]$R_{work} = \Sigma(||F_p(obs)| - |F_p(calc)||)/\Sigma |F_p(obs)|$; R_{free} is an R factor for a preselected subset (5%) of reflections that was not included in refinement.

Published September 14, 2015

Sey1p's G4 motif (R204 and D205) interact with the ribose of the nucleotide (Fig. S2 C) and are only seen in a subclass of the dynamin family that includes ATLs, Sey1p, RHD3, and GBPs. However, S68 in the P-loop of caSey1p is equivalent to S41 in Dynamin-1 (Chappie et al., 2010), which is required for GTP hydrolysis (Fig. S2, B and D). When compared with dynamin-1, the side chain of S68 does not point directly at the γ-phosphate bond of GTP and does not rotate during the transition state. Furthermore, a bridging sodium ion was found between S41 in dynamin-1 and the nucleotide (Fig. S2 D) but was not seen in Sey1p. In ATLs, an Arg finger (R77 in hsATL1) plays the same role at the position of S68 in caSey1p (Bian et al., 2011; Byrnes et al., 2013). This catalytic residue adopts a different rotamer conformation after the cleavage of the γ-phosphate bond, which in turn causes some minor local rearrangements (Fig. S2 D).

It is known that the GTPase activity of dynamin-1 is stimulated more than 100-fold, when self-assembled on lipid templates. Such dramatic increase was not seen with full-length scSey1p, when its GTPase activity in detergent was compared with that in reconstituted vesicles (Fig. S2 E). As expected and similar to dynamin-1, mutant S47A in scSey1p (equivalent to S68A in caSey1p) was less efficient in hydrolyzing GTP (Fig. S2 F). In addition, the side chain of caSey1p T95 and the backbone nitrogen of T94 and T95 engage the nucleotide. Consistent with the structural observations, mutation of scSey1p T75A (equivalent to T95A in caSey1p) reduces the enzymatic activity of the GTPase (Fig. S2, C and F).

Dimerization-induced membrane fusion

Nucleotide-dependent dimer formation is a common feature of dynamin-like GTPases. ATL dimerization is physiologically significant because ATL1 dimer mutants are defective in GTP hydrolysis and membrane fusion, and one "hot spot" of the hsATL1 mutations causing hereditary spastic paraplegia is localized in the GTPase domain near the dimer interface (Bian et al., 2011). Sey1p dimerization has been reported (Anwar et al., 2012) and was confirmed by our structural analysis (Fig. 1 B). Notably, hsATL1 dimers were seen in all structures, regardless of which nucleotide was added (GMP-PNP, GDP/AlF_4^-, and GDP), whereas caSey1p dimers only formed in the presence of GMP-PNP or GDP/AlF_4^-.

The dimerization of caSey1p involves a hydrophobic patch on top of the GTPase domain, including a conserved L257 (L233 in scSey1p and L274 in hsATL1) within the guanine cap, and several hydrophilic interactions along the GTPase interface (Fig. 2 A). The stalk domains also pack against each other in the dimer. The closest association was in 3HB-2: N407 and N410 from one molecule interact with K467 from the other, and E417 makes a salt bridge with K475 (Fig. 2 B). The bottoms of the stalk domains were also in proximity to each other. However, no substantial interactions were seen. The contact between the stalk domains occupies a surface area of 636 $Å^2$, despite the length of the domain. The overall dimer interface of caSey1p is 2891 $Å^2$, with a total surface area of 36269 $Å^2$ for each caSey1p molecule. In contrast, hsATL1 dimer buries 2,179 $Å^2$ in form 2 or 3,677 $Å^2$ in form 3 (with 949 $Å^2$ contributed by the 3HBs), even when the total surface area of each hsATL1 is ∼20,000 $Å^2$ and the 3HB being much shorter than the stalk domain of Sey1p.

To compare nucleotide-dependent dimerization of Sey1p and ATL, we performed analytical ultracentrifugation (AUC). As expected, purified cytSey1p from *S. cerevisiae* behaved as a monomer in the absence of nucleotide or in the presence of GDP, but it formed dimers in the presence of GMP-PNP or GDP/AlF_4^- (Fig. 2 C, left). Sedimentation equilibrium experiments revealed that the association of protomers was 57-fold stronger with GMP-PNP than with GDP/AlF_4^- (Fig. S3 A). In contrast, at the same protein concentration, cyt-hsATL1 exhibited much more stable dimer formation when GDP/AlF_4^- was present compared with GMP-PNP (Fig. 2 C, right; and Fig. S3 B). The same conclusion was drawn with the FRET-based assay (Liu et al., 2015). These results imply that, unlike ATL, Sey1p relies more on GTP binding than hydrolysis to achieve stable dimerization.

To probe the nucleotide requirement for Sey1p-mediated fusion, we used an in vitro lipid-mixing assay. In this assay, purified full-length scSey1p was reconstituted into donor and acceptor vesicles as judged by flotation experiments (Fig. S4 A). The donor vesicles contained lipids labeled with nitrobenzoxadiazole (NBD) and rhodamine at quenching concentrations; fusion with the unlabeled acceptor vesicles leads to fluorophore dilution and dequenching. Wild-type scSey1p resulted in efficient fusion in the presence of GTP and Mg^{2+}. No fusion was seen with GDP or in the absence of Mg^{2+} (Fig. 2 D). Interestingly, the addition of GMP-PNP caused moderate but reproducible fusion (Fig. 2 D). Such activity was not observed for *Drosophila* ATL (dmATL) in the presence of GMP-PNP or GDP/AlF_4^- (Fig. S4 C). Collectively, these results suggest that the linkage of opposing membranes through GTP binding-induced dimerization may be sufficient to promote Sey1p-mediated fusion.

To confirm that GTP binding without hydrolysis can cause fusion, we performed a visual assay of membrane tethering and fusion. Wild-type full-length scSey1p was reconstituted into vesicles containing phospholipids with either a fluorescent Oregon green or Rhodamine dye attached to the head groups. Samples of the reactions were diluted and visualized with a confocal microscope. The vesicles initially appeared as green or red punctae (Fig. 2 F, left). As recently reported for ATL, large yellow punctae (i.e., colocalization of the two dyes) appeared after the addition of GTP, indicating that the differently colored vesicles were associated or fused with one another (Fig. 2 F, middle). When EDTA, which chelates magnesium ions needed for nucleotide binding, was added, some of these large punctae disappeared or became smaller, indicating that some of the vesicles were untethered (Fig. 2 F, right). Very little tethering was seen in the presence of GDP/AlF_4^- (Fig. 2 H). In the presence of GMP-PNP, a low level of fusion was observed and was not strongly affected by EDTA addition (Fig. 2 G). These results confirmed that the addition of GMP-PNP promotes some Sey1p-mediated fusion.

Next, we tested the effect of dimer mutations on Sey1p activity. Mutation of L233 (equivalent to L257 in caSey1p shown in Fig. 2 A) drastically reduced the dimerization (Fig. S3 C), GTPase activity (Fig. S2 F), and fusion activity of scSey1p (Fig. 2 E and Fig. S4 B for reconstitution controls), whereas mutation of the corresponding L274 in ATL1 resulted in weaker defects in dimerization (Fig. S3 D). Deletion of 3HB-2 to 3HB-4 (residues 378–675) in the stalk domain (Δ3/4 stalk) of scSey1p, which abolishes most of the stalk interactions in the dimer and mimics the size of ATL1 (Fig. S1 C), strongly inhibited fusion activity (Fig. 2 E). scSey1p was also inactive when 3HB-2 was retained but 3HB-3 and -4 (residues 462–675) were truncated (Δ1/2 stalk; Fig. 2 E). Conversely, the removal of a long loop (residues 613–636) within 3HB-4 (ΔLoop) did not significantly affect fusion activity (Fig. 2 E). Nevertheless, all three mutations in the stalk domain had GTPase activity at wild-

Published September 14, 2015

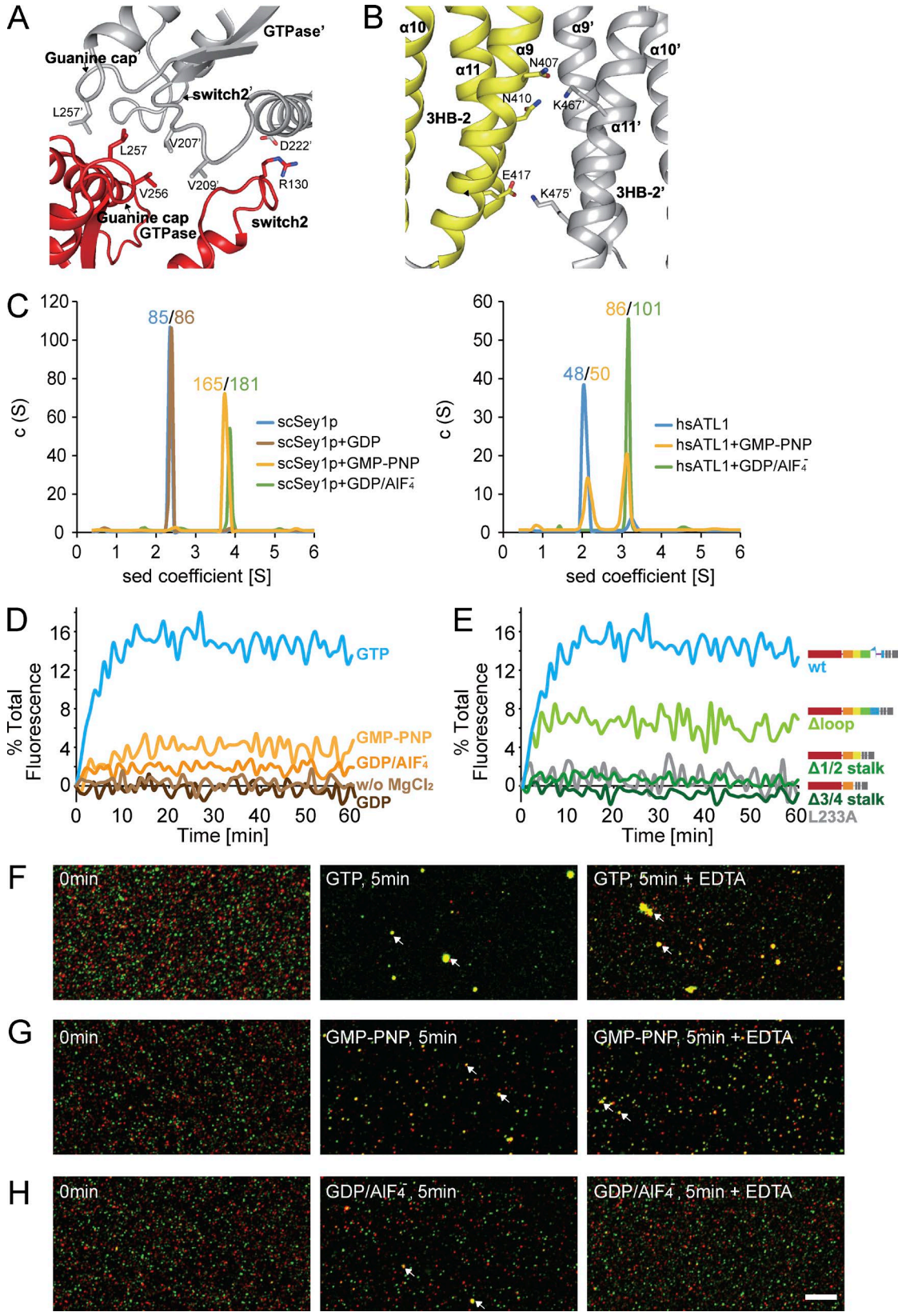

Figure 2. **Nucleotide-dependent dimerization of Sey1p.** (A) The interface between the two GTPase domains. The cartoon representation is colored as in Fig. 1. Key residues are indicated as sticks. The components of the second protomer (gray) are labeled with a prime symbol. (B) As in A, but for the interface between the two stalk domains. (C) The size of cyt-scSey1p (40 µM, theoretical molecular mass 80.8 kD) or cyt-hsATL1 (40 µM, theoretical molecular mass 51.7 kD) was determined by AUC in the presence of the indicated nucleotides. The estimated molecular masses are given above the peaks in kilodaltons. The data shown are from a single representative experiment out of three repeats. (D) Full-length wild-type (wt) scSey1p was reconstituted at equal concentrations into donor and acceptor vesicles (protein/lipid molar ratio of 1:200). Fusion of donor and acceptor vesicles was followed by the dequenching

Published September 14, 2015

type levels (Fig. S2 G). These results suggest that the length of the stalk domain is important for fusion.

Conformational change induced by P_i release

The structures suggest that Sey1p retains its configuration during hydrolysis of the γ-phosphate bond but undergoes at least two conformational changes upon P_i release: one in the active site and one involving repositioning of the stalk domain relative to the GTPase domain. In the GDP/AlF_4^- or GMP-PNP structure, switch 1 and 2 wrap around the nucleotide (Fig. 3 A). On the other hand, both loops are distant from the active site and partially disordered in the GDP structure (Fig. 3 A). These movements of switch 1 and 2 are typical among GTPases and explain why the dimer is stable with GMP-PNP or GDP/AlF_4^- but not with GDP, as the switches are at the dimerization interface (Figs. 2 A and 3 A).

Absence of the γ-phosphate not only breaks the caSey1p dimer but appears to alter the relative positions of the GTPase and stalk domains (Fig. 3 B). When GMP-PNP or GDP/AlF_4^- is bound, the linker connecting the GTPase domain and stalk domain attaches to the α7 of the other protomer. Major contacts include L312 and L318 from one molecule, and V319 and F322 from the other molecule (Fig. 3 C). In addition, Q315 forms a homotypic interaction, and D309 from the linker makes salt bridges to K323 and R376 of the other protomer (Fig. 3 C). In the GDP state, α7 docks to α6 of the same Sey1p molecule using mostly the same set of residues as in the GMP-PNP or GDP/AlF_4^- state. However, V319 and F322 engage M295 in α6, Q315 hydrogen bonds with Q303 and R299, and binding occurs between K323 and D291, and R376 and the carbonyl oxygen of A52 (Fig. 3 D).

A cross-linking assay was used to confirm the conformational change inferred from the structures. 3HB-1 of one cyt-Sey1p molecule and α6 of the other molecule came in proximity to one another in the presence of GMP-PNP or GDP/AlF_4^- but not GDP or in the absence of nucleotide. As expected, a cross-linked dimer formed when the scSey1p mutant L297C/V298C (L318C/V319C in caSey1p; see Fig. 3 C for positions of the mutations) was treated with diamide to induce disulfide bridge formation (Fig. 3 E, lanes 4 and 5 vs. 2 and 3). Cross-linked products were not observed when the scSey1p mutant M274C/V298C (M295C/V319C in caSey1p) was tested or when the reducing agent 2-mercaptoethanol was added (Fig. 3 E). Furthermore, as expected from the GDP/AlF_4^- and GMP-PNP structure in which residue N407 of one caSey1p molecule comes in proximity to K467 of the other caSey1p molecule (Fig. 2 B), cysteines introduced at these positions formed a disulfide bridge (Fig. 3 F, lanes 4 and 5). Finally, consistent with the AUC results, more dimers were formed with GMP-PNP than GDP/AlF_4^- (Fig. 3, E and F, compare lanes 4 and 5).

To directly assess whether the conformational changes are critical for fusion, we performed in vitro fusion assays. Mutation M274A in scSey1p (as M295A in caSey1p), which is predicted to play no role in dimerization and localizes to the GTPase-stalk interface in the GDP state, had reduced fusion activity comparable to the level of wild-type protein with GMP-PNP (Fig. 3 G). Similarly, mutant L297A in scSey1p (as L318A in caSey1p), which appears to be important for dimerization but not stabilization of the GDP state, was less effective in fusion (Fig. 3 H). Finally, substitution of V298 (as V319 in caSey1p) with ala, which disrupts GTPase–stalk interactions in both dimeric and monomeric conformations, drastically affected the fusion activity (Fig. 3 H). Collectively, these data strongly support the conformations observed in the structures.

Analysis of Sey1p in mammalian cells

To analyze the function of Sey1p, we tested whether it can replace ATLs in mammalian cells. We used siRNA to deplete the major ATL proteins, mainly ATL2 and ATL3 in COS-7 cells, and visualized the ER morphology using calreticulin as a marker. Consistent with previous results (Hu et al., 2009; Wu et al., 2015), when ATLs were knocked down in COS-7 cells (Fig. 4 A), the ER appeared as unbranched morphology in a majority of cells (Fig. 4, B and D), indicating defects in ER fusion. As expected, wild-type human ATL1, but not ATL1 with a mutation in the P-loop (K80A), efficiently restored the ER network in double-depleted cells (Fig. 4, C and D; and Fig. S5 A). When scSey1p was expressed at a comparable level, most cells had normal ER morphology (Fig. 4, C and D; and Fig. S5 A), suggesting that Sey1p and human ATL1 are equally active in maintaining the ER network. K50A (P-loop mutant), L233A (dimer interface mutant), L297A, V298A (both GTPase–stalk interface mutants), and Δ1/2stalk (stalk mutant) all failed to rescue the defects in ER morphology (Fig. 4 D and see Fig. S5 B for expression levels). Mutation M274A largely reduced the percentage of abnormal ER (Fig. 4 D), likely because it only affects the stabilization of the GDP-bound conformation and not Sey1p dimerization. These results confirm that Sey1p plays an important role in in the maintenance of ER morphology.

To test whether caSey1p and scSey1p have similar functions in cells, we expressed caSey1p in ATL-depleted COS-7 cells and monitored ER morphology (Fig. 4 C). As expected and similar to scSey1p, wild-type caSey1p but not GTP-binding defective mutant K71A successfully replaced ATLs in mammalian cells (Fig. 4, C and D). To further analyze the function of caSey1p, we expressed caSey1p under the control of the endogenous SEY1 promoter in a CEN vector (Fig. S5 C) in yeast cells lacking Sey1p and Yop1p, an ER tubule-forming protein, and exhibiting abnormal ER morphology. caSey1p was mostly capable of substituting scSey1p in the maintenance of ER morphology (Fig. S5 D). These results confirmed that caSey1p is a functional homologue of scSey1p.

Sey1p protein has been observed to be concentrated in punctae along the ER tubules in yeast cells, mainly at the three-way junctions of the tubules (Hu et al., 2009). The localization of scSey1p in COS-7 cells appears to be similar to that of yeast cells, regardless of whether ATLs are present (Figs. 4 C and 5 A). Punctae were also seen when caSey1p was expressed in ATL-depleted COS-7 cells (Fig. 4 C). Interestingly, scSey1p mutant with defective dimerization and fusion lost its punctate pattern (L233A;

of an NBD-labeled lipid present in the donor vesicles. Nucleotides, if indicated, were added at time 0. The data shown are from a single representative experiment out of four repeats. (E) As in D, but with stalk mutants. Δ3/4 stalk, deletion of residues 378–675 in scSey1p; Δ1/2 stalk, deletion of 462–675; ΔLoop, deletion of 613–636. The data shown are from a single representative experiment out of three repeats. (F) scSey1p-containing proteoliposomes, which also contained either Rhodamine- or Oregon green–labeled lipids, were mixed at a 1:1 ratio (total lipid concentration: 0.6 mM). One aliquot was analyzed immediately, a second was taken after incubation at 37°C with 1 mM GTP for 5 min, and a third was obtained after incubation with GTP followed by addition of 10 mM EDTA. All samples were diluted, spotted onto a coverslip, and visualized by confocal microscopy. Bar, 5 µm. (G) As in F, but with 1 mM GMP-PNP. (H) As in F, but with GDP/AlF_4^-. Arrows indicate tethered/fused vesicles.

Published September 14, 2015

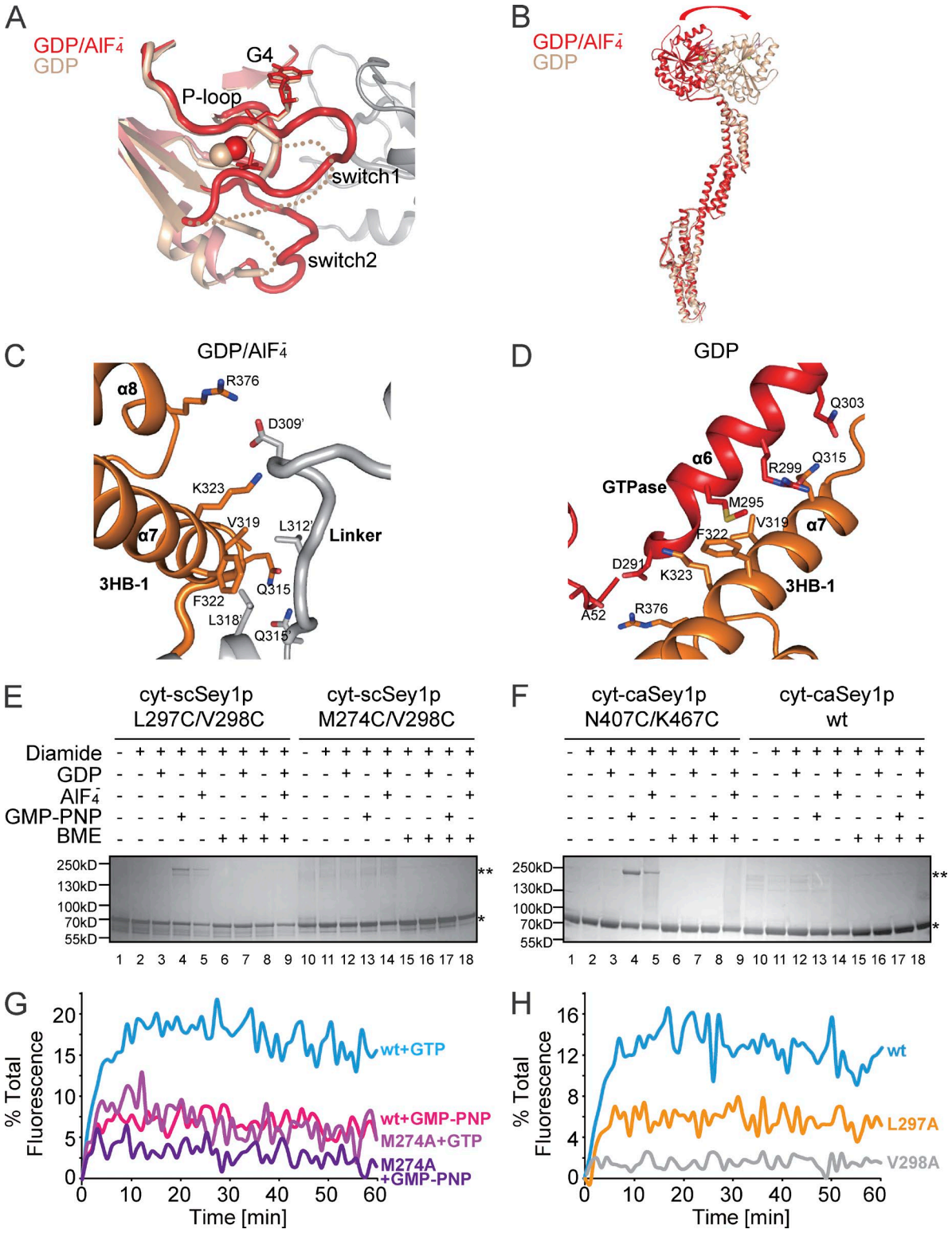

Figure 3. **Nucleotide-dependent conformational changes of Sey1p.** (A) Cartoon representation of the active site. The GDP/AlF_4^- state is colored in red and the GDP state in gold. The four signature motifs are highlighted. Note that switch 1 and switch 2 in the GDP state are partly disordered. The pairing protomer in the GDP/AlF_4^- state is shown in gray. (B) Superposition of the Sey1p structures in the GDP/AlF_4^- state (red) and the GDP state (gold). The movement of the GTPase domain is highlighted. (C) The GTPase-linker interface in the GDP/AlF_4^- state. The cartoon representation is colored as in Fig. 1. Key residues are shown in sticks. (D) As in C, but for the GTPase–stalk interface in the GDP state. (E) Purified cytosolic domains of scSey1p with cysteines at positions 297 and 298 or at positions 274 and 298 were treated with the oxidant diamide in the presence of the indicated nucleotides. Non–cross-linked protein (single asterisks) and cross-linked dimer (double asterisks) are indicated. Where indicated, the disulfide bridge was reduced with β-mercaptoethanol (BME) before nonreducing SDS/PAGE. (F) As in E, but with wild type (wt) or mutant (cysteines at positions 407 and 467) of the cytosolic domain of caSey1p. (G) Fusion assays of the M274A mutant of scSey1p. Wild-type samples were included for comparison. (H) As in G, but with the mutants of L297A and V298A. The data shown in G and H represents independent experiments with three independently purified batches of protein.

Published September 14, 2015

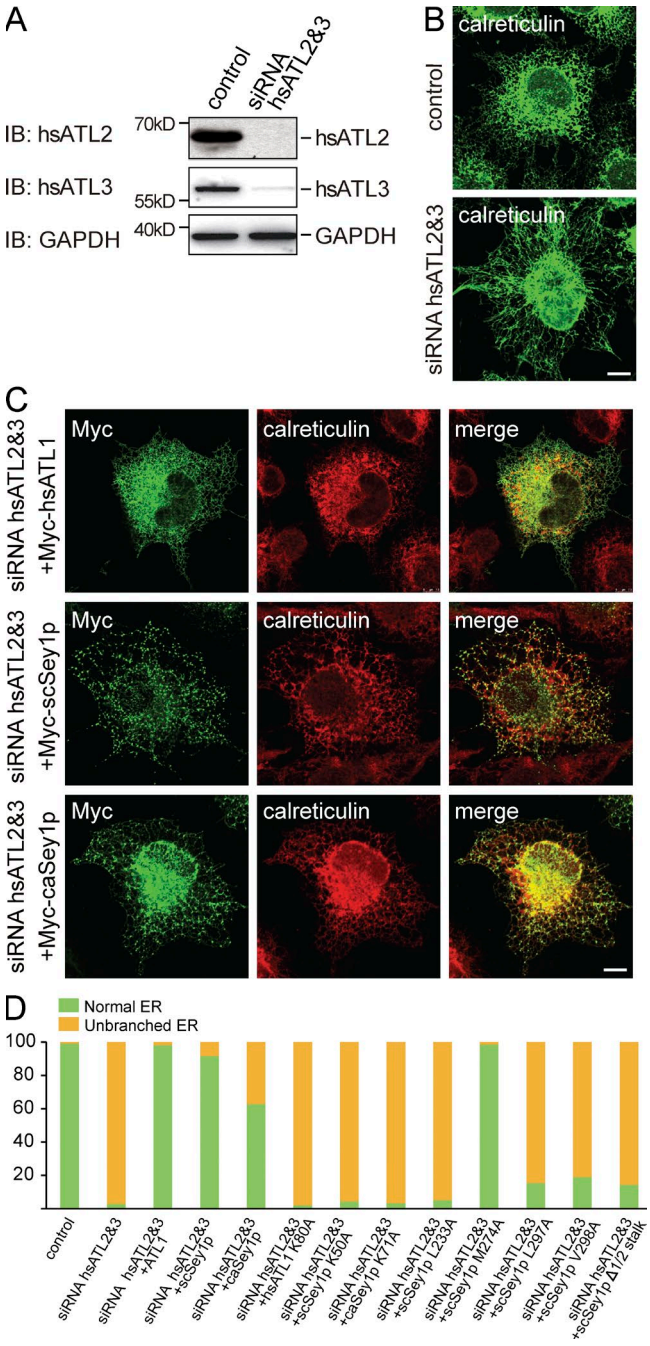

Figure 4. **Functional tests of Sey1p in cells.** (A) COS-7 cells were transfected with siRNA oligonucleotides against hsATL2 and 3. The levels of these proteins were determined by immunoblotting. GAPDH was used as a loading control. IB, immunoblot. (B) The ER morphology of COS-7 cells was visualized using calreticulin, an endogenous luminal ER protein, and indirect immunofluorescence using a confocal microscope. (C) Myc-hsATL1, Myc-scSey1p, or Myc-caSey1p was expressed in COS-7 cells and its localization determined by anti-Myc antibodies (green) and compared with that of calreticulin (red) using indirect immunofluorescence and confocal microscopy. (D) The ER morphology of indicated samples was categorized as "normal" (as in the top image of B) or "unbranched" (as in the bottom image of B). A total of 80–150 cells were counted for each sample. All graphs are representative of at least three repetitions. wt, wild type. Bars, 10 µm.

Fig. 5 B). ATL1 mainly distributed evenly along the ER tubules (Fig. 5 C), but ATL3 formed punctae like Sey1p (Fig. 5 D). Given that ATL3 was recently reported to be slower than ATL1 (Hu et al., 2015), GTPases with relatively low hydrolysis activity should tend to form punctae in cells. To test this possibility, we mutated the Arg finger of ATL1 (R77) to Ala. It has been reported that ATL1 R77A can still bind to GTP and form dimers, but GTP hydrolysis occurs much more slowly (Byrnes et al., 2013). We found that ATL1 R77A formed punctae in COS-7 cells (Fig. 5 E). The same results were obtained when these proteins were expressed in ATL-depleted cells (Fig. S5 B). These data suggest that punctae formation is dependent on GTPase activity.

Discussion

Our results suggest how Sey1p causes homotypic fusion of ER membranes (Fig. 6 A). First, two Sey1p molecules in different membranes bind GTP and form a dimer, thereby tethering the membranes together. It is possible that the stalk domains in the dimer do not associate initially but eventually reach the stable side-by-side conformation. To efficiently juxtapose the two membranes, we speculate that the Sey1p dimer does not come in between the membrane but rather sits on the orbit of two closely attached membrane regions with its GTPase domains pointing away from the tethered area. Flattened, closely spaced membranes were previously captured by cryo-EM during membrane tethering mediated by ATL or SNAREs (Diao et al., 2012; Hernandez et al., 2012; Saini et al., 2014). Multiple dimers may self-associate, perhaps through oligomerization of their TM regions and form a ring to stabilize the tethered state, during which time the two membranes begin to fuse. GTP hydrolysis and P_i release causes a conformational change, probably triggered by changes in the switch 1 region that is part of the GTPase domain dimer interface, and the switch 2 region that propagates at the interaction surface between the GTPase domain of one Sey1p molecule and the linker and stalk domain of the other. The GTPase domain would then be released and move freely until docking to its own stalk domain, resulting in disruption of the Sey1p dimer. Regardless of whether the membrane merging occurs before the monomerization of Sey1p, these molecules would start a new fusion attempt by searching for a dimer partner on opposing membranes.

Surprisingly, we observed membrane fusion by Sey1p even with GMP-PNP, indicating that fusion can occur without GTP hydrolysis. However, most of the Sey1p dimers formed with GMP-PNP would be on the same membrane, i.e., cis-dimer, and are futile. Fusion is much more efficient when GTP is added, as GTP hydrolysis would allow Sey1p cycling between dimer and monomer states. Consequently, more Sey1p monomers would be available for trans-interactions between different membranes. Such competition between cis- and trans-interactions has also been recently reported for ATL (Liu et al., 2015).

Sey1p- and ATL-mediated fusion differs in that the power stroke occurs at different steps of the GTP cycle. Stable trans-dimers of ATL (in form 3) are in a crossover configuration and would not be possible without GTP hydrolysis (Fig. 6 B). To achieve the tethered state, ATL molecules from apposing membranes have to bind GTP and dimerize into form 2 first; the two GTPase domains can then rotate and recapture the 3HBs from the pairing molecule to adopt form 3. The GTP-bound ATL dimer may switch between the two conformations until GTP hydrolysis drives the equilibrium toward form 3. Consistent

Published September 14, 2015

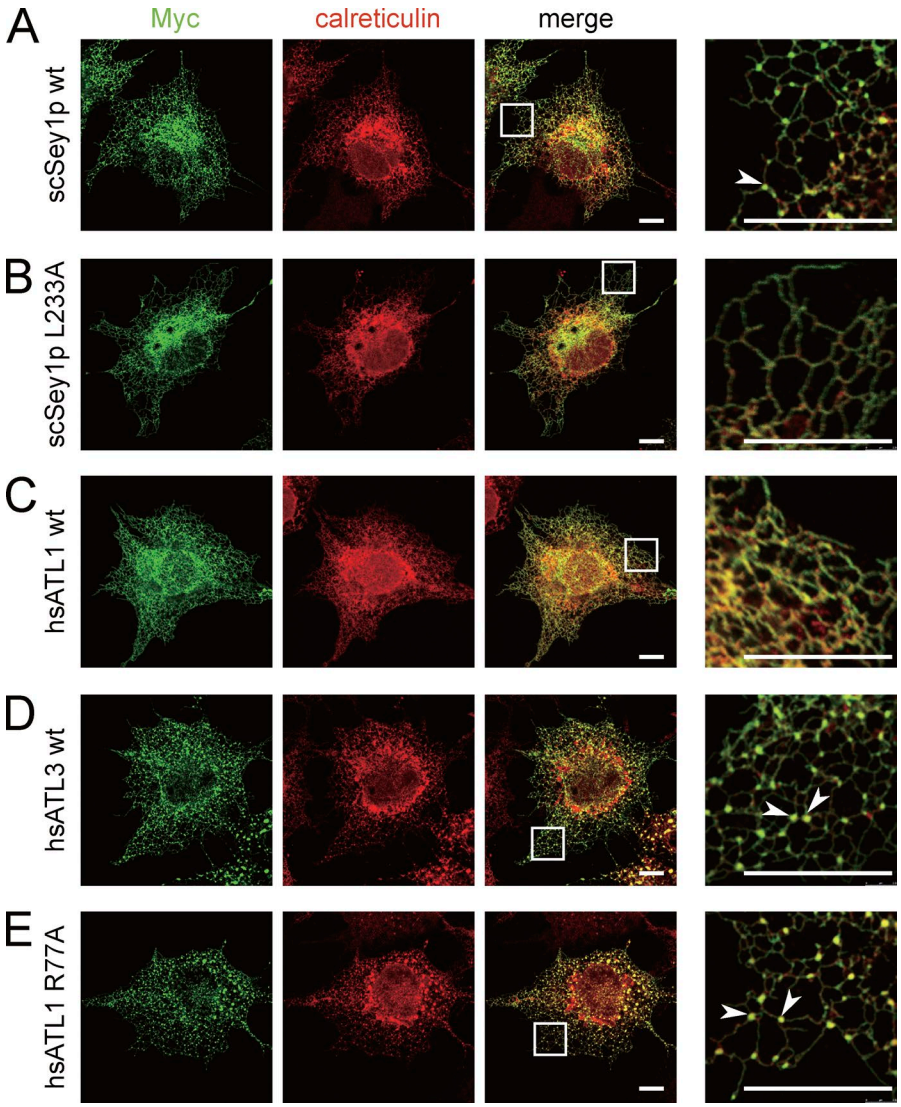

Figure 5. **Sey1p punctae formation.** (A) Myc-scSey1p was expressed in COS-7 cells and its localization determined by anti-Myc antibodies and compared with that of calreticulin using indirect immunofluorescence and confocal microscopy. The right image shows an enlargement of the boxed region centered on the tubular ER network. Bars, 10 µm. (B) As in A, but with cells expressing Myc-scSey1p L233A. (C) As in A, but with cells expressing Myc-hsATL1. (D) As in A, but with cells expressing Myc-hsATL3. (E) As in A, but with cells expressing Myc-hsATL1 R77A. The arrowheads indicate the puncta localized at the three-way junctions of the ER network.

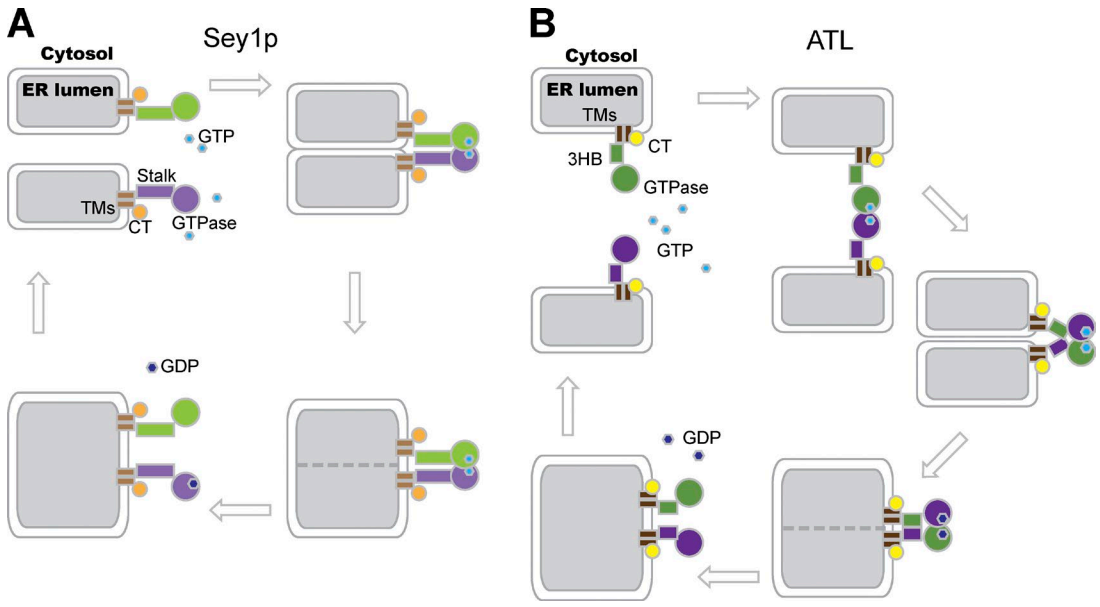

Figure 6. **Comparison of homotypic membrane fusion mediated by Sey1p and ATL.** (A) A model of Sey1p-mediated fusion. See Discussion for details. GTP and GDP molecules are indicated as cyan and blue spheres, respectively. (B) As in A, but for ATL. TMs, transmembrane segments; CT, cytosolic tail.

Published September 14, 2015

with these models, ATL dimer is most stable when in complex with GDP/AlF_4^-, whereas Sey1p dimer is strongest with GMP-PNP. Such a difference would not be explained by the structures but is likely determined by residues that sense the subtle change in distance between β- and γ-phosphate.

The formation of punctae at the three-way junctions or along ER tubules is seen in some, but not all, GTPase-based ER fusogens. Our results suggest that the kinetics of GTP hydrolysis play a role in punctae formation. Slow GTPases, such as Sey1p and ATL3, are prone to clustering. However, mutants with further reduced activity, which do not sustain fusion, will lose the punctate pattern and become evenly distributed on the ER membrane. One scenario would be that effective fusion requires the simultaneous participation of several GTPase molecules. Alternatively, slow hydrolysis would prolong the existence of a tethered complex, allowing the observation of punctae.

The proposed mechanism reveals that homotypic membrane fusion could be achieved by different approaches in Sey1p and ATL but with a similar paradigm. Some of the mechanism could apply to RHD3 and its homologues in the fusion of plant ER membranes, and to mitofusin/Fzo1p (Hermann et al., 1998; Chen et al., 2003), another member of the dynamin family, in the fusion of mitochondrial outer membranes. Three point mutations were previously identified in RHD3 (Wang et al., 1997). Based on sequence alignment with caSey1p, I134T and D185N would reside near the GTPase dimer interface, and A575V would be placed in the hydrophobic core of 3HB-4 (Fig. S1 D). The localization of these mutations confirms that dimerization of the GTPase domain and integrity of the stalk domain is critical for these dynamin-like proteins.

Materials and methods

Constructs, strains, and antibodies

The N-terminal cytosolic domains of *C. albicans* Sey1p (residues 1–692), codon-optimized *S. cerevisiae* Sey1p (residue 1–680), or hsATL1 (residues 18–447) were inserted into the NheI–XhoI sites of pET-28a (EMD Millipore), which includes a thrombin-cleavable, N-terminal 6×His-tag. For fusion assay, codon-optimized full-length scSey1p and full-length dmATL were cloned into the BamHI–XhoI sites of pGEX6p-1 vector with a GST tag followed by a PreScission protease digestion site at the N terminus. For mammalian expression, Myc-scSey1p, Myc-caSey1p, or Myc-hsATL1 was PCR-amplified and cloned into pcDNA4/TO (Invitrogen) by KpnI–BamHI, BamHI–XhoI, or KpnI–XhoI sites. Myc-hsATL3 was PCR amplified and cloned into pGW1. For endogenous level expression of scSey1p and caSey1p in yeast cells, the coding region of scSey1p and caSey1p plus an N-terminal HA tag and 300 bp upstream and downstream sequences of scSEY1 was amplified and inserted into the KpnI–NotI site of pRS316 (a URA/CEN plasmid). The plasmid pJK59, encoding Sec63-GFP was used to visualize ER morphology. All point mutations were generated using the QuikChange Site-Directed Mutagenesis kit (Agilent Technologies). The truncations (Δ3/4 stalk, deletion of residues 378–675 in scSey1p; Δ1/2 stalk, deletion of 462–675; ΔLoop, deletion of 613–636) were generated using overlap PCR primers. All constructs were confirmed by DNA sequencing.

The strain JHY4 (BY4741 *sey1Δ::kanMX4 yop1Δ::HIS3MX6*; Hu et al., 2009) was used to visualize ER morphology. Mouse anti-Myc and rabbit anti-Calreticulin antibodies were purchased from Abcam, and mouse anti-HA and mouse anti–phosphoglycerate kinase antibodies were purchased from Sigma-Aldrich.

Protein expression and purification

The cyt-caSey1p, cyt-scSey1p, and cyt-hsATL1 constructs were transformed into *Escherichia coli* strain BL21 (DE3), and cultures were grown in Luria-Bertani media at 37°C to an OD600 of 0.6. Protein expression was induced by the addition of 0.4 mM IPTG for 20 h at 16°C. Cells were harvested, resuspended in lysis buffer (20 mM Tris, pH 8.0, 150 mM NaCl, 4 mM $MgCl_2$, and 20 mM imidazole), and lysed by an ultra-high pressure cell disrupter (JN-3000 PLUS; JNBIO). The lysate was centrifuged at 16,000 rpm for 1 h, and the supernatant was collected. The protein was isolated by Ni-NTA chromatography (GE Healthcare) and further purified by ion-exchange chromatography (Resourse-Q or HiTrap Q; GE Healthcare) and gel filtration chromatography (Superdex-200; GE Healthcare). For crystallization, corresponding nucleotides at 2 mM were included in the gel filtration buffer (Yan et al., 2011; Chen et al., 2012).

For expression of selenomethionine-substituted (Se-Met) Sey1p, cells were grown in M9 medium at 37°C to an OD600 of 0.6. Solid amino acid supplements (50 mg/liter Lys, Thr, and Phe; 25 mg/liter Leu, Ile, and Val; 30 mg/liter Se-Met) were added to the medium before induction. The Se-Met protein was purified by the same procedure as the native protein.

Full-length dmATL or scSey1p were expressed and purified with a GST tag. The proteins were solubilized and isolated in Triton X-100 (Anatrace), and the GST tag was cleaved before reconstitution (Bian et al., 2011; Anwar et al., 2012).

X-ray crystallography

All native and selenomethionine-substituted proteins were concentrated to 8 mg/ml and crystallized by vapor diffusion methods at 16°C. Crystals of Sey1p with GDP/AlF_4^- were grown within days in 160 mM lithium sulfate monohydrate, 80 mM Tris, pH 8.5, 20% (wt/vol) polyethylene glycol (PEG) 3350, 40 mM ammonium acetate, 20 mM sodium citrate tribasic dehydrate, pH 5.6, 6% (wt/vol) PEG 4000, and 20 mM spermidine. Crystals of Sey1p with GMP-PNP appeared around 6 d in 120 mM DL-malic acid, pH 7.0, 16% (wt/vol) PEG 3350, 20 mM bicine, pH 9.0, 400 mM magnesium chloride hexahydrate, and 6% D-(+)-trehalose dihydrate. Crystals of Sey1p with GDP complex appeared around 2 mo in 20 mM Tris, pH 8.5, 160 mM potassium sodium tartrate tetrahydrate, 4 mM GDP, and 21% (wt/vol) PEG 3350.

All crystals were transferred to a cryo-protectant solution (4 M sodium formate) before being flash frozen in liquid nitrogen for storage. The native data for Sey1p with GDP was collected in a beamline BL17U at the Shanghai Synchrotron Radiation Facility (China). Other data were collected at 100 K using a charge-coupled device detector (Q270; Area Detector Systems Corporation) on beamline BL1A at Photon Factory (Japan). All data were processed and scaled using HKL2000 package 24 (Otwinowski and Minor, 1997).

The structure of Sey1p with GDP/AlF_4^- was solved by single anomalous diffraction of Se-Met using SHELX (Schneider and Sheldrick, 2002). An initial model was built by the program coot and used in molecular replacement to determine the structure of Sey1p with GDP or GMP-PNP (Emsley and Cowtan, 2004). For model refinement, the Phenix refinement program (phenix.refine) was used (Afonine et al., 2012). Interface and surface area was calculated using PDBePISA.

AUC

Purified cyt-scSey1p and cyt-hsATL1 were used for AUC in a buffer containing 50 mM Tris, pH 8.0, 300 mM NaCl, and 5 mM $MgCl_2$. Sedimentation velocity experiments were performed at 4°C in a proteomeLab XL-1 Protein Characterization System (Beckman Coulter). 2 mM GDP, 2 mM GMP-PNP, or 2 mM GDP/6 mM $AlCl_3$/30 mM NaF

Published September 14, 2015

were added to 40 µM protein before centrifugation. All interference data were collected at a speed of 42,000 rpm in a rotor (An-60 Ti; Beckman Coulter) and analyzed by the program SEDFIT in terms of a continuous c(s) distribution. In sedimentation equilibrium experiments, the proteins were prepared at three different concentrations (0.2, 0.3, and 0.5 mg/ml). Interference data were collected at three different speeds (8,000, 12,000, and 15,000 rpm for cytATL1; 6,400, 9,600, and12,000 rpm for cytSey1p) in a An-60 Ti rotor at 4°C and analyzed by SEDPHAT using a model of monomer–dimer self-association.

Cross-linking assays

1 µM wild-type or mutant cytSey1p protein in 50 mM Hepes, pH 7.4, 100 mM NaCl, and 5 mM $MgCl_2$ with or without 1 mM GDP, 1 mM GMP-PNP, or 1 mM GDP/3 mM $AlCl_3$/15 mM NaF was incubated with 10 µM diamide at room temperature for 30 min 500 µM *N*-ethylmaleimide was used to quench the reactions. The samples were analyzed by SDS-PAGE and Coomassie blue staining.

Fusion assays

Lipid-mixing assays were performed as previously described (Bian et al., 2011). In brief, lipids were dried down to a film, hydrated with A100 buffer (25 mM Hepes, pH 7.4, 100 mM KCl, 1 mM 2-mercaptoethanol, and 10% glycerol), and extruded through polycarbonate filters with a pore size of 100 nm. Proteins were reconstituted at a protein/lipid molar ratio of 1:200, except dmATL, which was reconstituted at a ratio of 1:1,000 (Fig. S4 C). The flotation of proteoliposomes was done on a sucrose gradient to determine the reconstitution efficiency. 20 mM proteoliposomes was mixed with 100 µl of 1.9 M sucrose and overlaid with 100 µl of 1.25 M sucrose and 30 µl of 0.25 M sucrose (all sucrose solutions were in 25 mM Hepes, pH 7.4, and 100 mM KCl). After centrifugation at 174,000 *g* for 75 min and 4°C in a rotor (TLS-55; Beckman Coulter), the gradient was fractionated into five fractions and analyzed by SDS-PAGE and Coomassie blue staining. Donor and acceptor liposomes were added at a 1:3 ratio. The initial NBD fluorescence was set to zero, and the maximum fluorescence was determined after addition of dodecyl maltoside.

Visual tethering/fusion assays

Full-length wild-type scSety1p was reconstituted into preformed liposomes with Rhodamine-DPPE (1,2-dipalmitoyl-sn-glycero-3-phosphoethanolamine) or Oregon green-DPPE (Invitrogen) in the same way as described in the methods of Fusion assays. The vesicles were mixed 1:1 in a reaction buffer containing 5 mM $MgCl_2$. Different nucleotides were added and the samples diluted 1:100 in reaction buffer or buffer with 10 mM EDTA. 5 µl samples were spotted onto a glass coverslip and visualized by confocal microscopy. Oregon green and Rhodamine dyes were excited with 488- and 561-nm lasers (100 mW), and their emissions selected with 530/40- and 620/50-nm filters, respectively. All images were captured under room temperature on a basic stand confocal microscope (AxioObsever Z1; Carl Zeiss) with a 63×/1.40 numerical aperture Plan Apochromat oil immersion objective lens using ZEN2012 software (Carl Zeiss). Changes were made linearly across the entire image using Photoshop (Adobe).

GTPase activity assays

GTPase activity assays were performed with the phosphate assay kit (Enzchek; Invitrogen). Reactions were performed in a 100 µl volume with 1 µM wild-type or mutant protein as indicated by the addition of 0.5 mM GTP. The absorbance at 360 nm was measured every minute over 30 min at 37°C using a micro-plate reader (Synergy 4; BioTek). The rate of phosphate release was calculated based on a standard curve.

Mammalian cell culture, transfections, and microscopy

COS-7 cells were maintained at 37°C with 5% CO_2 in DMEM containing 10% fetal bovine serum and passaged every 2–3 d. For siRNA transfections, COS-7 cells were plated at 50% confluency and transfected the next morning with 13 nM of each siRNA oligonucleotide duplex using RNAiMAX (Invitrogen) for 6 h. Cells were then scraped for immunoblot analysis or fixed for immunofluorescence analysis 48 h after transfection. Specific siRNA oligonucleotides (Invitrogen) for ATL2 were targeted against the following sequences: 5′-GGAGCUAUCCUUAUGAACAUUCAUA-3′; and that for ATL3 were 5′-GGUUAGAGAUUGGAGUUUCCCUUAU-3′. The control siRNA oligonucleotide was obtained from Invitrogen. The siRNA-resistant constructs were transfected into knockdown cells using Lipofectamine 3000 (Invitrogen) after 24 h of siRNA transfection.

Transfected cells were fixed for 20 min at room temperature with 4% formaldehyde (Bio Basic, Inc.) and permeabilized with 0.1% Triton X-100 (Bio Basic, Inc.). The cells were washed twice with PBS and probed with primary antibodies, including mouse anti-Myc antibody (Abcam) diluted 1:500 or rabbit anti-calreticulin antibody (Abcam) diluted 1:500, for 60 min in PBS containing 3% calf serum, followed by incubation with various fluorophore-conjugated secondary antibodies for an additional 45 min (Alexa Fluor 488–conjugated anti–rabbit or Alexa Fluor 594–conjugated anti–mouse (1:800 dilution; Invitrogen). For ER morphology rescue assay, yeast cells were imaged using Sec63p-GFP as a marker (Wu et al., 2015). All images were captured under room temperature on a confocal microscope (TCS SP5; Leica) with a 63×/1.40 numerical aperture Plan Apochromat oil immersion objective lens using LAS AF version 1.3.1 build 525 software (Leica).

Accession numbers

The coordinates and structure factors have been deposited in the Protein Data Bank under accession nos. 5CA8 (GDP bound state), 5CA9 (GDP/$AlF4^-$ bound state), and 5CB2 (GMP-PNP bound state).

Online supplemental material

Fig. S1 shows comparison of Sey1p and other dynamin-like proteins. Fig. S2 shows characterization of the GTPase domain of Sey1p. Fig. S3 shows AUC analysis of Sey1p and ATL1. Fig. S4 shows controls for fusion assay of Sey1p. Fig. S5 shows additional analysis of Sey1p in cells. Online supplemental material is available at http://www.jcb.org/cgi/content/full/jcb.201502078/DC1.

Ackowledgments

We thank T. Rapoport for critically reading the manuscript and the Tsinghua University Branch of China National Center for Protein Sciences (Beijing) for technical support.

L. Yan is a Tsinghua-Peking Center for Life Sciences postdoctoral fellow and is supported by the China Postdoctoral Science Foundation (2014M550713). Z. Lou is supported by the National Natural Science Foundation of China (grant 81322023) and the National Basic Research Program of China (973 Program, grants 2013CB911103 and 2014CB542802). J. Hu is supported by the National Natural Science Foundation of China (grant 31225006), the National Basic Research Program of China (973 Program, grant 2012CB910302), and an International Early Career Scientist grant from Howard Hughes Medical Institute.

The authors declare no competing financial interests.

Submitted: 20 February 2015
Accepted: 5 August 2015

Published September 14, 2015

References

Afonine, P.V., R.W. Grosse-Kunstleve, N. Echols, J.J. Headd, N.W. Moriarty, M. Mustyakimov, T.C. Terwilliger, A. Urzhumtsev, P.H. Zwart, and P.D. Adams. 2012. Towards automated crystallographic structure refinement with phenix.refine. *Acta Crystallogr. D Biol. Crystallogr.* 68:352–367. http://dx.doi.org/10.1107/S0907444912001308

Anwar, K., R.W. Klemm, A. Condon, K.N. Severin, M. Zhang, R. Ghirlando, J. Hu, T.A. Rapoport, and W.A. Prinz. 2012. The dynamin-like GTPase Sey1p mediates homotypic ER fusion in *S. cerevisiae*. *J. Cell Biol.* 197:209–217. http://dx.doi.org/10.1083/jcb.201111115

Bian, X., R.W. Klemm, T.Y. Liu, M. Zhang, S. Sun, X. Sui, X. Liu, T.A. Rapoport, and J. Hu. 2011. Structures of the atlastin GTPase provide insight into homotypic fusion of endoplasmic reticulum membranes. *Proc. Natl. Acad. Sci. USA.* 108:3976–3981. http://dx.doi.org/10.1073/pnas.1101643108

Byrnes, L.J., and H. Sondermann. 2011. Structural basis for the nucleotide-dependent dimerization of the large G protein atlastin-1/SPG3A. *Proc. Natl. Acad. Sci. USA.* 108:2216–2221. http://dx.doi.org/10.1073/pnas.1012792108

Byrnes, L.J., A. Singh, K. Szeto, N.M. Benvin, J.P. O'Donnell, W.R. Zipfel, and H. Sondermann. 2013. Structural basis for conformational switching and GTP loading of the large G protein atlastin. *EMBO J.* 32:369–384. http://dx.doi.org/10.1038/emboj.2012.353

Chappie, J.S., S. Acharya, M. Leonard, S.L. Schmid, and F. Dyda. 2010. G domain dimerization controls dynamin's assembly-stimulated GTPase activity. *Nature.* 465:435–440. http://dx.doi.org/10.1038/nature09032

Chen, H., S.A. Detmer, A.J. Ewald, E.E. Griffin, S.E. Fraser, and D.C. Chan. 2003. Mitofusins Mfn1 and Mfn2 coordinately regulate mitochondrial fusion and are essential for embryonic development. *J. Cell Biol.* 160:189–200. http://dx.doi.org/10.1083/jcb.200211046

Chen, J., G. Stefano, F. Brandizzi, and H. Zheng. 2011. *Arabidopsis* RHD3 mediates the generation of the tubular ER network and is required for Golgi distribution and motility in plant cells. *J. Cell Sci.* 124:2241–2252. http://dx.doi.org/10.1242/jcs.084624

Chen, X., X. Xu, Y. Sun, J. Zhou, Y. Ma, L. Yan, and Z. Lou. 2012. Purification, crystallization and preliminary X-ray crystallographic analysis of *Arabidopsis thaliana* dynamin-related protein 1A GTPase-GED fusion protein. *Acta Crystallogr. Sect. F Struct. Biol. Cryst. Commun.* 68:69–72. http://dx.doi.org/10.1107/S1744309111047634

Diao, J., P. Grob, D.J. Cipriano, M. Kyoung, Y. Zhang, S. Shah, A. Nguyen, M. Padolina, A. Srivastava, M. Vrljic, et al. 2012. Synaptic proteins promote calcium-triggered fast transition from point contact to full fusion. *eLife.* 1:e00109. http://dx.doi.org/10.7554/eLife.00109

Emsley, P., and K. Cowtan. 2004. Coot: model-building tools for molecular graphics. *Acta Crystallogr. D Biol. Crystallogr.* 60:2126–2132. http://dx.doi.org/10.1107/S0907444904019158

Faelber, K., Y. Posor, S. Gao, M. Held, Y. Roske, D. Schulze, V. Haucke, F. Noé, and O. Daumke. 2011. Crystal structure of nucleotide-free dynamin. *Nature.* 477:556–560. http://dx.doi.org/10.1038/nature10369

Faust, J.E., T. Desai, A. Verma, I. Ulengin, T.L. Sun, T.J. Moss, M.A. Betancourt-Solis, H.W. Huang, T. Lee, and J.A. McNew. 2015. The Atlastin C-terminal tail is an amphipathic helix that perturbs the bilayer structure during endoplasmic reticulum homotypic fusion. *J. Biol. Chem.* 290:4772–4783. http://dx.doi.org/10.1074/jbc.M114.601823

Ford, M.G., S. Jenni, and J. Nunnari. 2011. The crystal structure of dynamin. *Nature.* 477:561–566. http://dx.doi.org/10.1038/nature10441

Ghosh, A., G.J. Praefcke, L. Renault, A. Wittinghofer, and C. Herrmann. 2006. How guanylate-binding proteins achieve assembly-stimulated processive cleavage of GTP to GMP. *Nature.* 440:101–104. http://dx.doi.org/10.1038/nature04510

Hermann, G.J., J.W. Thatcher, J.P. Mills, K.G. Hales, M.T. Fuller, J. Nunnari, and J.M. Shaw. 1998. Mitochondrial fusion in yeast requires the transmembrane GTPase Fzo1p. *J. Cell Biol.* 143:359–373. http://dx.doi.org/10.1083/jcb.143.2.359

Hernandez, J.M., A. Stein, E. Behrmann, D. Riedel, A. Cypionka, Z. Farsi, P.J. Walla, S. Raunser, and R. Jahn. 2012. Membrane fusion intermediates via directional and full assembly of the SNARE complex. *Science.* 336:1581–1584. http://dx.doi.org/10.1126/science.1221976

Hu, J., Y. Shibata, P.P. Zhu, C. Voss, N. Rismanchi, W.A. Prinz, T.A. Rapoport, and C. Blackstone. 2009. A class of dynamin-like GTPases involved in the generation of the tubular ER network. *Cell.* 138:549–561. http://dx.doi.org/10.1016/j.cell.2009.05.025

Hu, J., W.A. Prinz, and T.A. Rapoport. 2011. Weaving the web of ER tubules. *Cell.* 147:1226–1231. http://dx.doi.org/10.1016/j.cell.2011.11.022

Hu, X., F. Wu, S. Sun, W. Yu, and J. Hu. 2015. Human atlastin GTPases mediate differentiated fusion of endoplasmic reticulum membranes. *Protein Cell.* 6:307–311. http://dx.doi.org/10.1007/s13238-015-0139-3

Lee, Y., D. Paik, S. Bang, J. Kang, B. Chun, S. Lee, E. Bae, J. Chung, and J. Kim. 2008. Loss of spastic paraplegia gene atlastin induces age-dependent death of dopaminergic neurons in *Drosophila*. *Neurobiol. Aging.* 29:84–94. http://dx.doi.org/10.1016/j.neurobiolaging.2006.09.004

Lee, M., S.K. Paik, M.J. Lee, Y.J. Kim, S. Kim, M. Nahm, S.J. Oh, H.M. Kim, J. Yim, C.J. Lee, et al. 2009. *Drosophila* Atlastin regulates the stability of muscle microtubules and is required for synapse development. *Dev. Biol.* 330:250–262. http://dx.doi.org/10.1016/j.ydbio.2009.03.019

Lin, S., S. Sun, and J. Hu. 2012. Molecular basis for sculpting the endoplasmic reticulum membrane. *Int. J. Biochem. Cell Biol.* 44:1436–1443. http://dx.doi.org/10.1016/j.biocel.2012.05.013

Liu, T.Y., X. Bian, S. Sun, X. Hu, R.W. Klemm, W.A. Prinz, T.A. Rapoport, and J. Hu. 2012. Lipid interaction of the C terminus and association of the transmembrane segments facilitate atlastin-mediated homotypic endoplasmic reticulum fusion. *Proc. Natl. Acad. Sci. USA.* 109:E2146–E2154. http://dx.doi.org/10.1073/pnas.1208385109

Liu, T.Y., X. Bian, F.B. Romano, T. Shemesh, T.A. Rapoport, and J. Hu. 2015. Cis and trans interactions between atlastin molecules during membrane fusion. *Proc. Natl. Acad. Sci. USA.* 112:E1851–E1860. http://dx.doi.org/10.1073/pnas.1504368112

Low, H.H., and J. Löwe. 2006. A bacterial dynamin-like protein. *Nature.* 444:766–769. http://dx.doi.org/10.1038/nature05312

Low, H.H., C. Sachse, L.A. Amos, and J. Löwe. 2009. Structure of a bacterial dynamin-like protein lipid tube provides a mechanism for assembly and membrane curving. *Cell.* 139:1342–1352. http://dx.doi.org/10.1016/j.cell.2009.11.003

Orso, G., D. Pendin, S. Liu, J. Tosetto, T.J. Moss, J.E. Faust, M. Micaroni, A. Egorova, A. Martinuzzi, J.A. McNew, and A. Daga. 2009. Homotypic fusion of ER membranes requires the dynamin-like GTPase atlastin. *Nature.* 460:978–983. http://dx.doi.org/10.1038/nature08280

Otwinowski, Z., and W. Minor. 1997. Processing of X-ray diffraction data collected in oscillation mode. *Methods Enzymol.* 276:307–326. http://dx.doi.org/10.1016/S0076-6879(97)76066-X

Saini, S.G., C. Liu, P. Zhang, and T.H. Lee. 2014. Membrane tethering by the atlastin GTPase depends on GTP hydrolysis but not on forming the cross-over configuration. *Mol. Biol. Cell.* 25:3942–3953. http://dx.doi.org/10.1091/mbc.E14-08-1284

Salinas, S., C. Proukakis, A. Crosby, and T.T. Warner. 2008. Hereditary spastic paraplegia: clinical features and pathogenetic mechanisms. *Lancet Neurol.* 7:1127–1138. http://dx.doi.org/10.1016/S1474-4422(08)70258-8

Schiefelbein, J.W., and C. Somerville. 1990. Genetic control of root hair development in *Arabidopsis thaliana*. *Plant Cell.* 2:235–243. http://dx.doi.org/10.1105/tpc.2.3.235

Schneider, T.R., and G.M. Sheldrick. 2002. Substructure solution with SHELXD. *Acta Crystallogr. D Biol. Crystallogr.* 58:1772–1779. http://dx.doi.org/10.1107/S0907444902011678

Shibata, Y., G.K. Voeltz, and T.A. Rapoport. 2006. Rough sheets and smooth tubules. *Cell.* 126:435–439. http://dx.doi.org/10.1016/j.cell.2006.07.019

Stefano, G., L. Renna, T. Moss, J.A. McNew, and F. Brandizzi. 2012. In *Arabidopsis*, the spatial and dynamic organization of the endoplasmic reticulum and Golgi apparatus is influenced by the integrity of the C-terminal domain of RHD3, a non-essential GTPase. *Plant J.* 69:957–966. http://dx.doi.org/10.1111/j.1365-313X.2011.04846.x

Wang, H., S.K. Lockwood, M.F. Hoeltzel, and J.W. Schiefelbein. 1997. The ROOT HAIR DEFECTIVE3 gene encodes an evolutionarily conserved protein with GTP-binding motifs and is required for regulated cell enlargement in *Arabidopsis*. *Genes Dev.* 11:799–811. http://dx.doi.org/10.1101/gad.11.6.799

Wu, F., X. Hu, X. Bian, X. Liu, and J. Hu. 2015. Comparison of human and *Drosophila* atlastin GTPases. *Protein Cell.* 6:139–146. http://dx.doi.org/10.1007/s13238-014-0118-0

Yamada-Okabe, T., and H. Yamada-Okabe. 2002. Characterization of the CaNAG3, CaNAG4, and CaNAG6 genes of the pathogenic fungus *Candida albicans*: possible involvement of these genes in the susceptibilities of cytotoxic agents. *FEMS Microbiol. Lett.* 212:15–21. http://dx.doi.org/10.1111/j.1574-6968.2002.tb11238.x

Yan, L., Y. Ma, Y. Sun, J. Gao, X. Chen, J. Liu, C. Wang, Z. Rao, and Z. Lou. 2011. Structural basis for mechanochemical role of *Arabidopsis thaliana* dynamin-related protein in membrane fission. *J. Mol. Cell Biol.* 3:378–381. http://dx.doi.org/10.1093/jmcb/mjr032

Zhang, M., F. Wu, J. Shi, Y. Zhu, Z. Zhu, Q. Gong, and J. Hu. 2013. ROOT HAIR DEFECTIVE3 family of dynamin-like GTPases mediates homotypic endoplasmic reticulum fusion and is essential for *Arabidopsis* development. *Plant Physiol.* 163:713–720. http://dx.doi.org/10.1104/pp.113.224501

Zhao, X., D. Alvarado, S. Rainier, R. Lemons, P. Hedera, C.H. Weber, T. Tukel, M. Apak, T. Heiman-Patterson, L. Ming, et al. 2001. Mutations in a newly identified GTPase gene cause autosomal dominant hereditary spastic paraplegia. *Nat. Genet.* 29:326–331. http://dx.doi.org/10.1038/ng758